Laser and Particle Beams (2008), *26*, 661–670. Printed in the USA.

doi:10.1017/S0263034608000682

Angular distribution and conversion of multi-keV L-shell X-ray sources produced from nanosecond laser irradiated thick-foil targets

G.-Y. HU,[1,2,3] J.-Y. ZHANG,[2] J. ZHENG,[3] B.-F. SHEN,[1] S.-Y. LIU,[2] J.-M. YANG,[2] Y.-K. DING,[2] X. HU,[2] Y.-X. HUANG,[2] H.-B. DU,[2] R.-Q. YI,[2] A.-L. LEI,[1] AND Z.-Z. XU[1]

[1]State Key Laboratory of High Field Laser Physics, Shanghai Institute of Optics and Fine Mechanics, CAS, Shanghai, China
[2]Research Center of Laser Fusion, CAEP, Mianyang, China
[3]CAS Key Laboratory of Basic Plasma Physics, Department of Modern Physics, University of Science and Technology of China, Hefei, China

(RECEIVED 1 August 2008; ACCEPTED 1 October 2008)

Abstract

An experimental study on the angular distribution and conversion of multi-keV X-ray sources produced from 2 ns-duration 527nm laser irradiated thick-foil targets on Shenguang II laser facility (SG-II) is reported. The angular distributions measured in front of the targets can be fitted with the function of $f(\theta) = \alpha + (1-\alpha)\cos^{\beta}\theta$ (θ is the viewing angle relative to the target normal), where $\alpha = 0.41 \pm 0.014$, $\beta = 0.77 \pm 0.04$ for Ti K-shell X-ray sources (~4.75 keV for Ti K-shell), and $\alpha = 0.085 \pm 0.06$, $\beta = 0.59 \pm 0.07$ for Ag/Pd/Mo L-shell X-ray sources (2–2.8 keV for Mo L-shell, 2.8–3.5 keV for Pd L-shell, and 3–3.8 keV for Ag L-shell). The isotropy of the angular distribution of L-shell emission is worse than that of the K-shell emission at larger viewing angle (>70°), due to its larger optical depth (stronger self-absorption) in the cold plasma side lobe surrounding the central emission region, and in the central hot plasma region (emission region). There is no observable difference in the angular distributions of the L-shell X-ray emission among Ag, Pd, and Mo. The conversion efficiency of Ag/Pd/Mo L-shell X-ray sources is higher than that of the Ti K-shell X-ray sources, but the gain relative to the K-shell emission is not as high as that by using short pulse lasers. The conversion efficiency of the L-shell X-ray sources decreases with increasing atomic numbers (or X-ray photon energy), similar to the behavior of the K-shell X-ray source.

Keywords: Angular distribution; Laser plasma; X-ray source

INTRODUCTION

Multi-keV X-ray sources are widely used in the fields of high energy density physics (HEDP) and inertial confinement fusion (ICF) as backlighting beam (Kalantar *et al.*, 1997; Pikuz *et al.*, 2002; Rafique *et al.*, 2008), probe beam (Glenzer *et al.*, 2003; Riley *et al.*, 2007; Schollmeier *et al.*, 2006; Abdallah *et al.*, 2007; Faenov *et al.*, 2007; Wong *et al.*, 2007), or heating beam (Glenzer *et al.*, 2003; Riley *et al.*, 2002*a*) for the diagnostics or the production of high density plasmas (Tahir *et al.*, 2004, 2007; Schollmeier *et al.*, 2008). The detailed characteristics of multi-keV X-ray emission are important to optimize X-ray sources or design experiments. Most of the articles concerning this issue concentrate on the influence of the laser intensity (Mattews *et al.*, 1983; Workman *et al.*, 2003; Workman & Kyrala, 2001*a*, 2001*b*; Riley *et al.*, 2002*b*; Dunn *et al.*, 1995; Kodama *et al.*, 1986), the atomic number (Kauffman, 1991; Mattews *et al.*, 1983; Workman & Kyrala, 2001*a*, 2001*b*; Dunn *et al.*, 1995; Ruggles *et al.*, 2003; Yaakobi *et al.*, 1981; Kodama *et al.*, 1986), and the initial density of the target (Back *et al.*, 2001, 2003; Fiedorowicz, 2005; Fournier *et al.*, 2004, 2006; Kodama *et al.*, 1987; Teubner *et al.*, 1991; Pelletier *et al.*, 1997; Girard *et al.*, 2005, 2004; Primout, 2005). Some papers pay attention to the influence of the laser focus spot size (Mattews *et al.*, 1983; Workman *et al.*, 2003; Workman & Kyrala, 2001*a*, 2001*b*; Riley *et al.*, 2002*b*), the laser wavelength (Kauffman, 1991; Hu *et al.*, 2008; Mattews *et al.*,

Address correspondence and reprint requests to: G.Y. Hu, State Key Laboratory of High Field Laser Physics, Shanghai Institute of Optics and Fine Mechanics, CAS, Shanghai 201800, China. E-mail: gyhu@siom.ac.cn

1983; Yaakobi *et al.*, 1981; Kodama *et al.*, 1986), the laser incidence angle (Mattews *et al.*, 1983), or the laser pulse duration (Mattews *et al.*, 1983; Workman & Kyrala, 2001*a*, 2001*b*; Riley *et al.*, 2002*b*; Dunn *et al.*, 1995; Phillion & Hailey, 1986; Kodama *et al.*, 1987; Teubner *et al.*, 1991; Pelletier *et al.*, 1997; Girard *et al.*, 2004; Eidmann & Schwanda, 1991; Limpouch *et al.*, 2002; Von Der Linde *et al.*, 2001), etc. We also found that by using a long pulse laser, the laser focus spot size and the thickness of the thin-foil target (the thickness is comparable to the burn through length, which is the initial target thickness that the laser beam can transmit through the entire plasma region with little absorption at the end of the laser pulse) can change the conversion of multi-keV K-shell X-ray emission significantly (Hu *et al.*, 2007, 2008).

However, relatively little experimental work has been dedicated to the angular distribution of multi-keV X-ray emission, which is necessary in order to explore the physical process of laser target coupling (Max, 1982), test hydrodynamic codes (Girard *et al.*, 2004), and design the experiment (Kalantar *et al.*, 1997; Pikuz *et al.*, 2002; Glenzer *et al.*, 2003; Riley *et al.*, 2002a, 2007; Schollmeier *et al.*, 2006). Many parameters can effect the angular distribution such as target material, laser wavelength, laser pulse duration, X-ray photon energy, and other factors. X-ray angular distributions have been explored mainly in the region of extreme ultraviolet (EUV) and sub-keV X-ray emission (Higashiguchi *et al.*, 2006; Kodama *et al.*, 1986; Celliers *et al.*, 1996; Mead *et al.*, 1981, 1983). A few papers paid attention to the angular distribution of multi-keV X-ray emission of Al, Mg K-shell emission (Chase *et al.*, 1977; Arora *et al.*, 2001). Additional experiments are needed to study the angular distribution of multi-keV X-ray emission sources produced with the widely used target materials in nowadays experiments of HEDP and ICF. In this article, we measured the angular distribution of multi-keV K- and L-shell X-ray emission (~4.75 keV for Ti K-shell, 3–3.8 keV for Ag, 2.8–3.5 keV for Pd, and 2–2.8 keV for Mo L-shell) produced by 2 ns-duration 527 nm laser irradiated thick-foil target (the thickness is much larger than the burn through length) (Hu *et al.*, 2008).

With long pulse laser beams, the measurements of the conversion efficiency of multi-keV X-ray sources were focused on the K- and M-shell emission in the past (Kauffman, 1991; Babonneau, 1999). Multi-keV L-shell X-ray sources produced with long pulse laser irradiated solid targets have been used frequently as heating or backlighting sources (Pikuz *et al.*, 2002; Glenzer *et al.*, 2003; Riley *et al.*, 2007; Schollmeier *et al.*, 2006; Riley *et al.*, 2002*a*; Glendinning *et al.*, 1995; Scott *et al.*, 2001). The conversion efficiency of multi-keV L-shell X-ray sources have mainly been explored with short pulse laser beams (Kauffman, 1991; Phillion & Hailey, 1986; Glendinning *et al.*, 1995; Eidmann & Schwanda, 1991). A few papers explored the multi-keV L-shell emission with long pulse laser (Eidmann & Schwanda, 1991; Mochizuki & Yamanaka, 1986; Glibert *et al.*, 1980). The hydrodynamic behavior of multi-keV L-shell X-ray emission region with long pulse laser beams is different to that with short pulse laser beams, which (the difference of the hydrodynamic behavior) will change the conversion efficiency of X-ray source (Kauffman, 1991; Phillion & Hailey, 1986; Glendinning *et al.*, 1995). In this article, we explored the conversion of the L-shell multi-keV X-ray emission in the laser parameters range different to that in the previous papers (Eidmann & Schwanda, 1991; Mochizuki & Yamanaka, 1986; Glibert *et al.*, 1980). The conversion efficiency of Ag/Pd/Mo L-shell X-ray sources is obviously higher than that of the Ti K-shell X-ray sources, which is benefited from the wider spectral bandwidth of L-shell emission relative to that of the K-shell emission.

EXPERIMENTAL SETUP

The experiment is performed at the Shenguang II (SG-II) laser facility (Lin *et al.*, 1999) located at the Shanghai Institute of Optics and Fine Mechanics (SIOM). The schematic setup of the experiment is shown in Figure 1. The Beam #9 (Peng *et al.*, 2006) laser beam (~1.5 kJ, ~2 ns, 527 nm, $f/4.5$) irradiates solid targets at an incidence angle of either 22.5° or 0°. The solid targets are titanium (^{22}Ti) foil of 6 μm thickness, silver (^{47}Ag), palladium (^{46}Pd), or molybdenum (^{42}Mo) foils

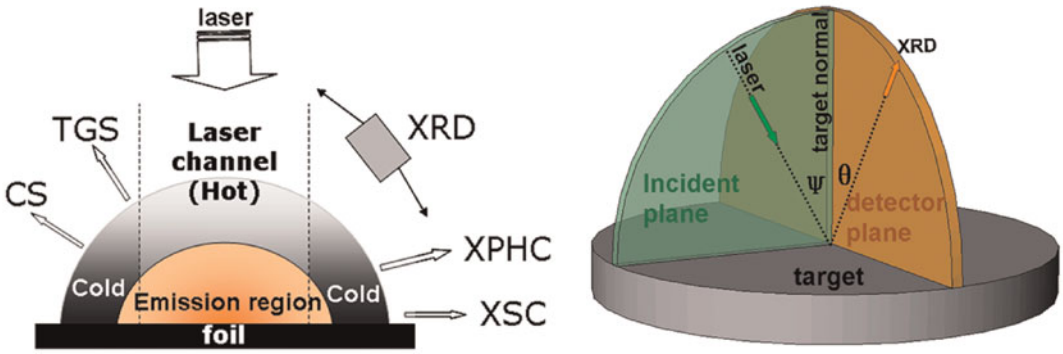

Fig. 1. (Color online) Experimental setup and the sketch map of the emission region, the hot laser channel (central hot plasma region), and the cold plasma side lobe surrounding the emission region (left). The schematic view of the laser incidence plane and the detector plane (right). Ψ and θ are respectively the laser incidence angle and the viewing angle of detector relative to the target normal.

https://doi.org/10.1017/S0263034608000682 Published online by Cambridge University Press

Table 1. *The 2ns-duration laser parameters (the laser energy, the incidence angle, and the size of the focus spot. φ is the diameter (FWHM) of the circular focus spot)*

Ti	Ag	Pd	Mo
1380J/0^0/φ350 μm (smoothed)	1920J/22.5^0/φ260 μm (defocused)	1560J/22.5^0/φ350 μm (smoothed)	1360J/45^0/φ350 μm (defocused)
1660J/22.5^0/φ350 μm (smoothed)	1290J/22.5^0/φ230 μm (defocused)	1440J/22.5^0/φ230 μm (defocused)	NA
1400J/0^0/400 μm × 400 μm (smoothed)	1350J/22.5^0/φ230 μm (defocused)	1050J/22.5^0/φ350 μm (smoothed)	NA

of 2 μm thickness. In the shots with Mo target, the incidence angle is 45°. The laser energy changes in the range from 1 kJ to 1.9 kJ in our experiment, as shown in Table 1. The laser beam is focused on the target front with a circular spot of about 350 μm full width at half maximum (FWHM) diameter, or a 400 μm × 400 μm (FWHM) quadrate spot after being smoothed with a lens array (Deng *et al.*, 1986), or defocused to about 230–260 μm diameter (FWHM) circular spot without the lens array (the laser focus spot point at some place behind the target).

The diagnostic system is similar to that in our previous work (Hu *et al.*, 2007, 2008). A set of X-ray diodes (XRDs) at different viewing angles are used to give the X-ray flux and the angular distribution with temporal resolution of 250 ps and relative uncertainty of ±30%. The stability of the XRDs is ±10% among different shots. The azimuth angles of XRD are perpendicular to the laser incidence plane, as shown in Figure 1. With appropriate filters, only the K- or L-shell X-rays that we are interested in, as shown in Figure 3b, can be detected by the XRDs (>4 keV for Ti, >2.5 keV for Ag/Pd, and >2 keV for Mo). We also use other assistant detectors, such as an X-ray pinhole camera (XPHC), gives the time-integrated multi-keV X-ray emission region, an X-ray streak pinhole camera (XSC), gives the one-dimensional motions of the multi-keV X-ray emission region around the target axis, a crystal spectrometer (CS), gives the detailed spectrum of K- and L-shell emission recorded on image plate using polyethylene terephthalate (PET) or titanium alkyl phosphates (TIAP) crystal, and a 2000 line/mm transmission grating spectrometer (TGS), gives the whole X-ray spectrum included soft and multi-keV emission recorded on CCD.

A stainless-steel washer with 50 μm thickness was used to hold the foil (500 μm inner diameter and 1200 μm outer diameter for circular focus spot, and 1200 μm inner diameter and 2000 μm outer diameter for 400 μm ×400 μm quadrate focus spot). In the shots of detecting the angular distribution in Figure 4, one quarter of the target washer was removed and all of the XRDs are at the side of the 90° gap to avoid the shadow of the target washer. But in the shots of Figure 2, there is no gap on the target washer, which induced the horizontal shadows in Figures 2c and 2d.

EMISSION REGION AND X-RAY SPECTRUM

When the laser beam irradiates the thick-foil target, the ablated hot plasma expands along the target normal in one dimension first. Then the central hot plasma will expand laterally and form side lobe plasma surrounding the central hot plasma. At the same time, the X-ray emission comes from the central hot plasma will evaporate the off-spot material and enhance the forming of the side lobe plasma. The effect of the radiation cooling will lower the temperature of the side lobe plasma substantially. Then the plasma region comes to a quasi-steady state (the plasma conditions change very slow) with a central hot plasma region (we call it laser channel in this article) surrounded by a cold plasma side lobe outside the laser-irradiated target region. After several nanoseconds, the pressure balances in the lateral direction, the plasma will form a density depression on axis and a significant cold plasma side lobe. The detailed physical process can be seen elsewhere (Filevich *et al.*, 2003).

In our experiments, the laser pulse duration is not long enough to establish the pressure balance completely; the ablated plasma will just come to a quasi-steady state since the plasma conditions change very slowly, the density depression on axis is not significant. Generally, the quasi-steady state will be obtained when the longitudinal size of the coronal plasma is close to two times the size of the focus spot (Max, 1982; Labate *et al.*, 2005). Then the multi-keV X-ray emission region and the multi-keV X-ray flux will evolve into quasi-steady state because the multi-keV X-rays come from the central hot plasma region (hot underdense coronal plasma zone). In the quasi-steady state, the longitudinal size of the emission region becomes comparable to the size of the focus spot because the multi-keV X-ray flux is proportional to $n_e^2 T_e$ (n_e and T_e are electron density and temperature, respectively) (Labate *et al.*, 2005; Montgomery *et al.*, 1994; Batha *et al.*, 1995; Hu *et al.*, 2007, 2008). The transverse dimension (FWHM) of the emission region also comes to quasi-steady state with a size slightly larger than that of the focus spot due to the effect of lateral energy transport and radiation cooling (Filevich *et al.*, 2003). This phenomenon is found for various focus spot size (Hu *et al.*, 2008), and for various target materials. As shown in Figure 2, the transverse dimension and the evolvement of the longitudinal size of the emission region (Hu *et al.*, 2007, 2008) have no difference between the Ti K-shell emission and Ag L-shell emission before and after (>1 ns) the appearance of the quasi-steady state, which indicate that in the case of thick solid target irradiated by long pulse laser, the emission region with the same

https://doi.org/10.1017/S0263034608000682 Published online by Cambridge University Press

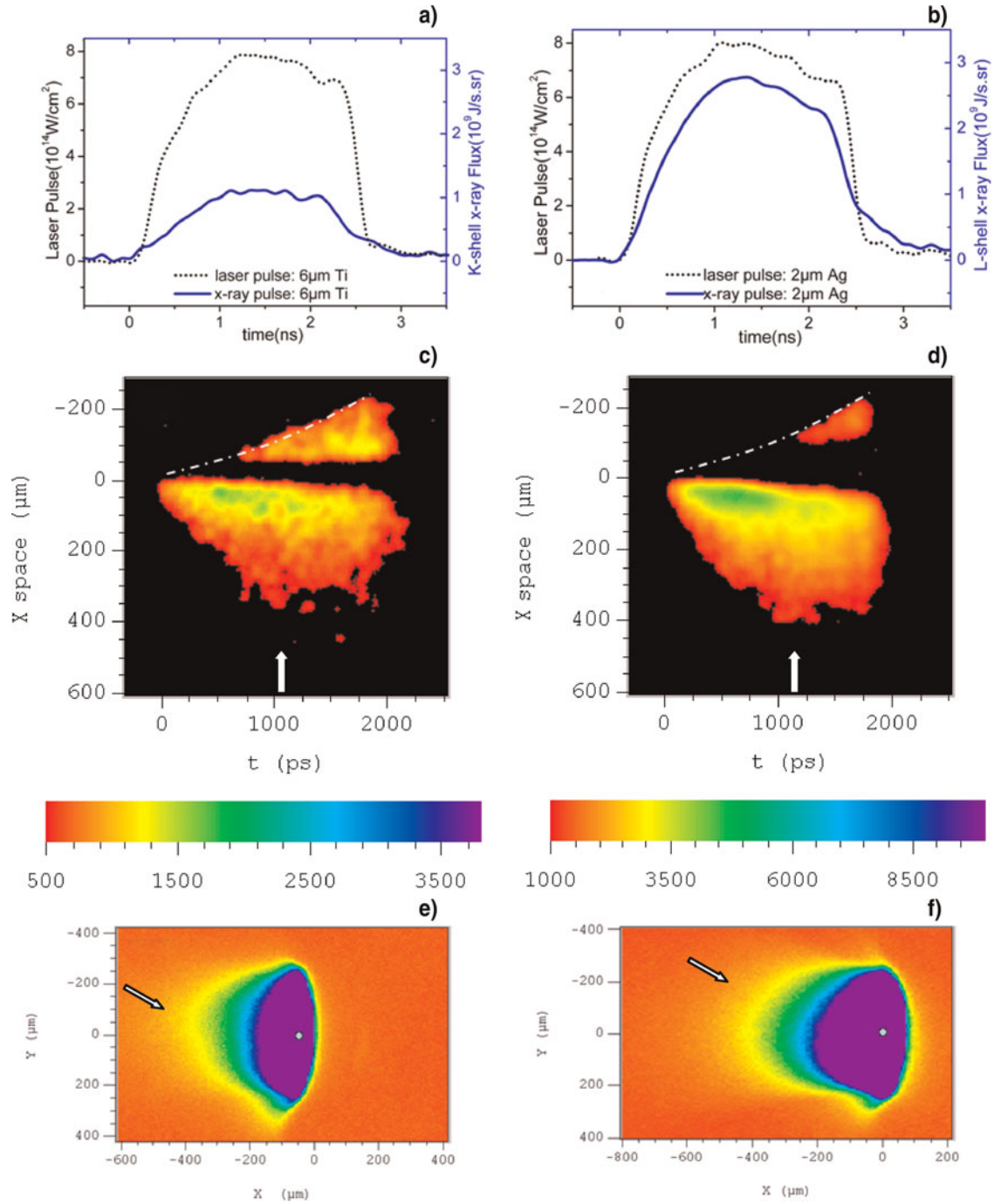

Fig. 2. (Color online) (**a**, **b**) The laser pulse and X-ray flux given by XRD at 0° viewing angle relative to the target normal, (**c**, **d**) the longitudinal temporal profile of the emission region given by XSC, (**e**, **f**) the time integrated images of emission region given by XPHC at 76° viewing angle relative to the target normal. The laser parameters for the Ti K-shell emission (>4 keV) in (a, c, e) are 1.6 kJ energy, 2 ns duration, 22.5° incidence angle, and 350 μm diameter (FWHM) focus spot smoothed with a lens arrays, and the laser parameters for the Ag L-shell emission (>2.5 keV) in (b, d, f) are 1.7 kJ energy, 2 ns duration, 22.5° incidence angle, and 350 μm diameter (FWHM) focus spot smoothed with a lens arrays. The horizontal shadows in (c, d) are due to the washer of the targets. The white arrows in (c, d, e, f) show the incidence direction of laser pulse. The white points in (e, f) indicate the target center. The central zones in (e, f) are saturated, so the real longitudinal scale length of the emission region should refer to (c, d).

laser focus spot will remain the same size for various target materials.

The detailed spectra of the Ti K-shell and the Pd, Ag L-shell emission given by CS are shown in Figure 3a. The influences of the diffraction efficiency of crystal and the spectral response efficiency of imaging plate have not been considered. The spectral bandwidth of the L-shell emission spectrum is obviously wider than that of the K-shell emission

https://doi.org/10.1017/S0263034608000682 Published online by Cambridge University Press

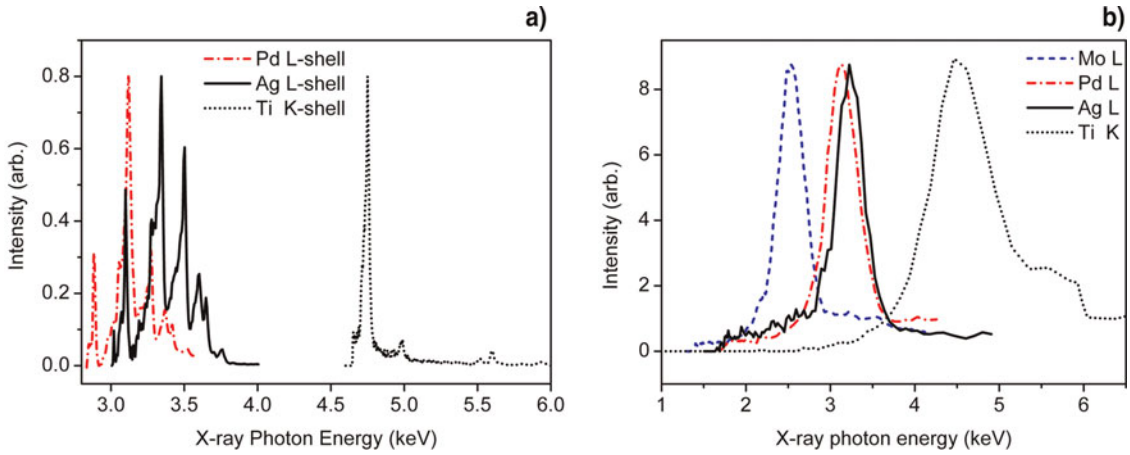

Fig. 3. (Color online) The detailed X-ray spectra (**a**) and rough X-ray spectra (**b**) given by CS and TGS respectively. The relative spectral bandwidth in (b) is useless because the spectral resolution of TGS for Ti K-shell emission is different to that of the Mo/Pd/Ag L-shell emission.

due to the larger number of charge-state configurations and transition lines, which will increase the conversion efficiency of the L-shell X-ray source (Kauffman, 1991), and the phenomenon is shown in Figure 5. The rough emission spectra given by TGS are shown in Figure 3b, which have been modified with the transmission function of the filters used on the XRD (the original spectra given by TGS multiplied with the transmission function of the filters used on the XRD). It indicates that the X-ray photon energy that can enter the XRD are >4 keV for Ti, >2.5 keV for Ag/Pd, and >2 keV for Mo, which mainly come from the corresponding K- or L-shell line emission as shown in Figure 3a.

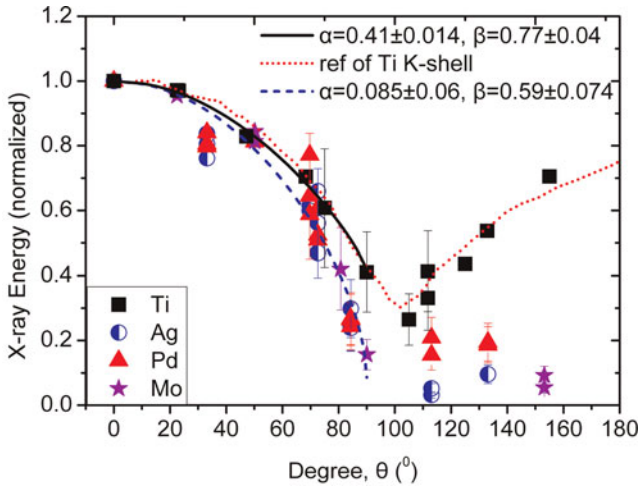

Fig. 4. (Color online) The angular distribution of multi-keV Ti K-shell and Ag/Pd/Mo L-shell X-ray emission. The black solid line and blue short dash line are the fitting curves for K- and L-shell emission respectively with the function of $f(\theta) = \alpha + (1 - \alpha) \cos^{\beta} \theta$. The red short-dot line (ref) is given by 2D hydrodynamic simulation code FCI2 for Ti K-shell emission (Girard *et al.*, 2004). The relative uncertainty of the X-ray energy is ±30%. The 2ns-duration laser parameters are shown in Table 1.

ANGULAR DISTRIBUTION

The angular distributions of Mo/Pd/Ag L-shell emission and Ti K-shell emission are shown in Figure 4. The laser conditions are shown in Table 1. The viewing angles are relative to the target normal as shown in Figure 1. All of the data were normalized with the maximal value given by the XRD at the viewing angle near the target normal. To keep the visibility of the figure, not all of the error bars of ±30% is added in Figure 4. With the same target material, the differences of the angular distributions between various shots are not significant, which indicates that the effects of laser intensity and focus spot size on the angular distribution are not significant in our experiment. So we add the experimental data of three shots to one profile in the case of Ti, Ag, and Pd targets. The method can increase the density of data points and decrease the influence of the stochastic fluctuation of the data to the fitting. Within the error range, there are no notable differences between the measured angular distribution of Ag, Pd, and Mo L-shell emission in front of the target as shown in Figure 4, so we can fit the angular distribution of Ag/Pd/Mo L-shell emission with the same function. The angular distribution behind the target is beyond the scope of the present paper because it is also influenced by the target thickness. We just consider the angular distribution in front of the target.

Usually the multi-keV X-ray emission is reduced away from the target normal but not zero at the 90° viewing angle, which is perpendicular to the target normal, so we can fit the data in front of the target roughly with the function of $f(\theta) = \alpha + (1-\alpha) \cos^{\beta} \theta$, where $f(\theta)$ is the X-ray energy detected by the XRD at some viewing angle normalized with the maximal X-ray energy value given by the XRD at the viewing angle near the target normal, θ is the viewing angle relative to the target normal. We found that the fitting index of K-shell emission are $\alpha = 0.41 \pm 0.014$,

https://doi.org/10.1017/S0263034608000682 Published online by Cambridge University Press

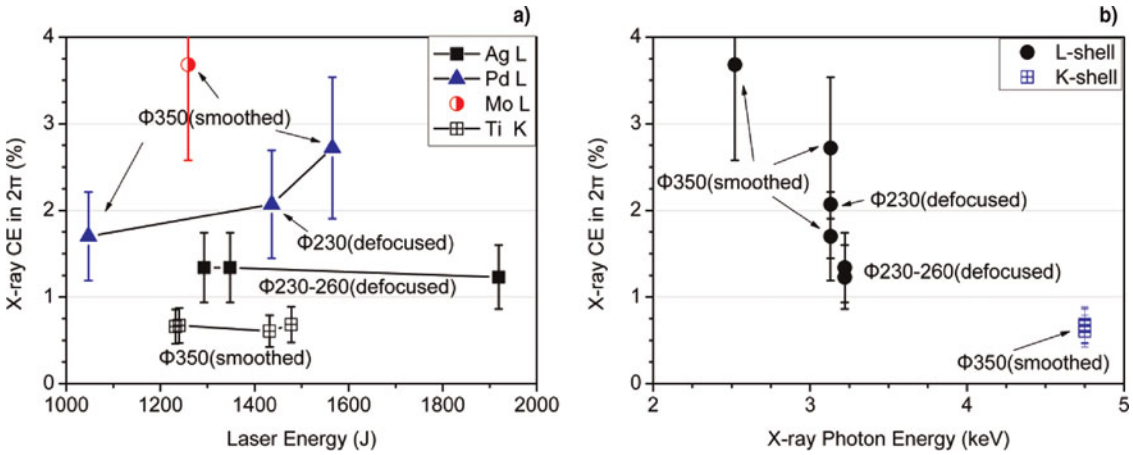

Fig. 5. (Color online) The X-ray conversion efficiency (CE) of Ti K-shell and Ag/Pd/Mo L-shell emission versus laser energy (**a**) and X-ray photon energy (**b**). The laser parameters for Ag, Pd, and Mo are shown in Table 1. The data of Ti K-shell emission of 6 μm thick target with 22.5° incidence angle are taken from the reference of Hu *et al.* (2007).

$\beta = 0.77 \pm 0.04$, and the fitting index of L-shell emission are $\alpha = 0.085 \pm 0.06$, $\beta = 0.59 \pm 0.074$. The fitting index of L-shell emission is similar to that of Au soft X-ray emission calculated with LASNEX (150 μm diameter focus spot and 600-ps laser pulse) (Mead *et al.*, 1981). In Figure 4, the two-dimensional hydrodynamic code FCI2 simulation result for the angular distribution of Ti K-shell emission (Girard *et al.*, 2004) was also shown. The simulation result is in good agreement with our experimental data, which indicates that the reliable angular distribution can be obtained with the two-dimensional hydrodynamic simulation code FCI2. The slight difference may be induced by the different laser incidence angle between the simulation setting and our experiment.

It is evident from the experimental data and the fitting function in Figure 4 that the X-ray energy decreases away from the target normal, and the isotropy of the L-shell emission is slightly worse than that of the K-shell emission at large viewing angle (>70°). The multi-keV X-ray emission region locates in the central hot plasma region (laser channel), and it is always surrounded by the cold plasma side lobe outside the laser channel that does not emit multi-keV X-rays before and after the coming of the quasi-steady state (Filevich *et al.*, 2003). When the X-rays emitted by the central hot emission traverse through the cold surrounding plasma side lobe, it will be absorbed partially. Because the density of the surrounding cold plasma side lobe descends exponentially away from the target, the area density (plasma density multiplied by length) of the cold plasma side lobe where the multi-keV X-rays traverse increases with the increasing of the viewing angle relative to the target normal, which will increase the absorption and reduce the X-ray energy that enters the detector. So the X-ray energy will decrease with the increasing of the viewing angle relative to the target normal. In the cold plasma side lobe surrounding the emission region, the optical depth of the L-shell emission is larger than that of the K-shell emission, which will increase the absorption, so the isotropy of the L-shell emission is slightly worse than that of the K-shell emission at larger viewing angle. The optical depth of the Ag, Pd, and Mo L-shell emission in the cold plasma is approximately the same for the corresponding target materials of Ag, Pd, and Mo, so there are no obvious differences between the angular distributions of L-shell emission. Besides the self-absorption in the surrounding cold plasma side lobe, the self-absorption in the central hot plasma region can also effect the angular distribution of multi-keV X-rays. But the self-absorption in the central hot plasma region is not as strong as that in the cold plasma side lobe because the temperature of the central hot plasma is very high.

With the fitted angular distribution, the relative total X-ray energies are 0.74 and 0.66 of that obtained with the assumption of isotropy emission for K- and L-shell emission, respectively (Hu *et al.*, 2007). The decrease of the X-ray energy at large viewing angle is serious compared to that at the 0° viewing angle, the effect of the angular distribution should be considered carefully in experiments using the X-ray source at large viewing angle (Kalantar *et al.*, 1997; Pikuz *et al.*, 2002; Glenzer *et al.*, 2003; Riley *et al.*, 2002*b*, 2007; Schollmeier *et al.*, 2006).

It should be noticed that the measured angular distribution of X-ray emission is influenced not only by the viewing angle of the detector relative to the target normal, but also possibly by the laser incidence angle. But in our experiments, the influence of laser incidence angle can not be distinguished due to the small variation range of the incidence angle (0° and 22.5°). Although in the shots of Mo target, the incidence angle is 45°, but unfortunately there is just one kind of incidence angle with Mo target and we can not compare it with that of other incidence angle. We will explore this problem in the future.

https://doi.org/10.1017/S0263034608000682 Published online by Cambridge University Press

CONVERSION EFFICIENCY

In this article, the X-ray energy CE is defined as the total multi-keV X-ray energy in 2π space in front of the target (>4 keV for Ti K-shell emission, >2.5 keV for Ag/Pd, and >2 keV for Mo L-shell emission, as shown in Fig. 3b) divided by the laser energy, which is different from that of our previous article (Hu *et al.*, 2007). We use the data given by the XRD nearest to the target normal and the fitting function of the angular distribution of K- and L-shell emission to calculate the total X-ray energy and the conversion efficiency.

Figure 5 shows the CE of K- and L-shell X-ray emission measured with XRD. The CEs are 0.6%–0.7% for Ti K-shell emission with 350 μm diameter (FWHM) smoothed circular focus spot, which is smaller than that obtained with the assumption of isotropy emission in 4π space significantly (Hu *et al.*, 2007), 1.2%–1.4% for Ag L-shell emission with 230–260 μm diameter (FWHM) defocused circular focus spot, 1.7%–2.7% for Pd L-shell emission with 230 μm diameter (FWHM) defocused or 350 μm diameter (FWHM) smoothed circular focus spot, and 3.7% for Mo L-shell emission with 350 μm diameter (FWHM) smoothed circular focus spot. The CE of the Pd L-shell emission increases with the laser energy. It's very strange respect with that of the Ti K-shell and Ag L-shell emission. The reason is not clear. Maybe the laser intensity for Pd is near to the optimized laser intensity, similar to that in the work of Workman *et al.* (2003).

The CE of Ag/Pd/Mo L-shell emission is significantly higher than that of the Ti K-shell emission. As shown in Figure 2, it is not induced by the change of the size of the emission region, so it should be because of the atomic transition process. First, the L-shell emission with larger number of charge-state configurations has more transition channels relative to that of the K-shell emission, represented by the more transition lines and wider spectral bandwidth as shown in Figure 3a, which can increase the transition probability and the emission energy (Kauffman, 1991). Second, with the same temperature, the transition with lower X-ray photon energy of 2–4 keV Ag/Pd/Mo L-shell emission has more population in the higher level relative to that of the >4 keV Ti K-shell emission, which can increase the photon number and the emission power (Griem, 1997). Those two factors enhance the CE of the Ag/Pd/Mo L-shell emission relative to that of the Ti K-shell emission.

The gain of the CE of the L-shell emission relative to that of the K-shell emission using long pulse laser beam in our experiment is not as high as that of using short pulse laser (Kauffman, 1991; Phillion & Hailey, 1986). The CE of the Pd L-shell emission is about 29–31 times that of the Ti K-shell emission with 120 ps or 60 ps short pulse laser (Kauffman, 1991; Phillion & Hailey, 1986), but in our experiment with the 2 ns-duration long pulse laser, the gain is just 2.8–4.5. This phenomenon was also found in other experiments (Mochizuki & Yamanaka, 1986; Glibert *et al.*, 1980). In the case of short pulse laser (Kauffman, 1991; Phillion & Hailey, 1986), not only the difference of the charge-state configurations, but also the difference of the hydrodynamic behavior, which determine the volume of the emission region, will influence the conversion of the L-shell emission relative to that of the K-shell emission. But with the long pulse laser in our experiment, the coronal plasma that emits multi-keV X-rays and the volume of the emission region remains the same for various target material as shown in Figure 2 (Hu *et al.*, 2007, 2008), only the difference of the charge-state configurations will benefit the conversion of the L-shell emission. So, with a long pulse laser beam, the gain of the CE of the Ag/Pd/Mo L-shell emission relative to that of the Ti K-shell emission is not as high as that with a short pulse laser.

For the L-shell emission, the CE increases steadily with the decrease of the X-ray photon energy and target atomic number, which is similar to the behavior of K-shell emission (Kauffman, 1991; Ruggles *et al.*, 2003; Workman & Kyrala, 2001*a*, 2001b). In the same row in the periodic table of the elements and with the same temperature, the lower X-ray photon energy (smaller atomic number) with the lower transition energy has more population in the higher level, which can increase the photon number and the emission energy. In accordance with bound-bound and bound-free emissivity behavior, the CE can be scaled as $T_e^{1/2}\exp(-h\nu/T_e)$ approximately ($h\nu$ is the X-ray photon energy) (Griem, 1997), where T_e can be estimated with the analytic theory (Fabbro *et al.*, 1985). But in our experiment, the data have not the same laser parameters, such as the laser focus spot and beam smoothing etc, which will change the CE markedly (Hu *et al.*, 2007, 2008). So, we can not give a reliable scaling rule of CE as a function of X-ray photon energy that is suitable for the whole L-shell emission range in our experiment.

CONCLUSION

The angular distributions of multi-keV X-ray sources produced by long pulse laser irradiated thick-foil target are measured and can be fitted with the function of $f(\theta) = \alpha + (1 - \alpha)\cos^{\beta}\theta$, where $\alpha = 0.41 \pm 0.014$, $\beta = 0.77 \pm 0.04$ for Ti K-shell emission, and $\alpha = 0.085 \pm 0.06$, $\beta = 0.059 \pm 0.74$, for Mo/Pd/Ag L-shell emission, respectively. The K-shell emission, with smaller optical depth in the cold plasma side lobe surrounding the emission region and in the central hot plasma region, is closer to isotropy distribution than L-shell emission. There are no significant differences between the angular distributions of Ag, Pd, and Mo L-shell emission. With long pulse laser, the X-ray conversion efficiency of the Ag/Pd/Mo L-shell emission is significantly higher than that of the Ti K-shell emission, but the gain relative to the K-shell X-ray emission is not as high as that with short pulse laser (Kauffman, 1991; Phillion & Hailey, 1986). The X-ray conversion efficiency of the L-shell emission increases with the decreasing of the X-ray photon energy

https://doi.org/10.1017/S0263034608000682 Published online by Cambridge University Press

and atomic number, which is similar to the behavior of the K-shell emission (Kauffman, 1991; Ruggles *et al.*, 2003; Workman, & Kyrala, 2001*a*, 2001*b*).

ACKNOWLEDGEMENTS

The authors are grateful to the SG-II laser operation group and the target fabrication group for their laborious work and close collaboration. This work was supported by the National High Technology Programs on Inertial Confinement Fusion, Science and Technology Development Fund of CAEP under Grant No. 2007B08003, National Natural Science Foundation of China under Grant Nos. 10375064, 10625523, and 10775165, and National Basic Research Program of China (973 Program) under Grant No. 2006CB806000.

REFERENCES

Abdallah, J., Batani, D., Desai, T., Lucchini, G., Faenov, A., Pikuz, T., Magunov, A. & Narayanan, V. (2007). High resolution X-ray emission spectra from picosecond laser irradiated Ge targets. *Laser Part. Beams* **25**, 245–252.

Arora, V., Chakera, J.A., Kumbhare, S.R., Naik, P.A., Gupta, N.K. & Gupta, P.D. (2001). Angular distribution of X-ray line radiation from laser-irradiated planar targets. *Laser Part. Beams* **19**, 253–257.

Babonneau, D., Bonnet, L., Jacquemot, S., Bocher, J.L., Boutin, J.Y., Jadaud, J.P. & Vilette, B. (1999). X-ray conversion with PHEBUS laser. *Laser Part. Beams* **17**, 459–463.

Back, C.A., Grun, J., Decker, C., Suter, L.J., Davis, J., Landen, O.L., Wallace, R., Hsing, W.W., Laming, J.M., Feldman, U., Miller, M.C. & Wuest, C. (2001). Efficient multi-keV underdense laser-produced plasma radiators. *Phys. Rev. Lett.* **87**, 275003.

Back, C.A., Grun, J., Decker, C., Suter, L.J., Davis, J., Landen, O.L., Wallace, R., Hsing, W.W., Laming, J.M., Feldman, U., Miller, M.C. & Wuest, C. (2003). Multi-keV X-ray conversion efficiency in laser-produced plasmas. *Phys. Plasmas* **10**, 2047–2055.

Batha, S.H., Procassini, R.J., Hammel, B.A., Shepard, T.D., Drake, R.P., Bradley, K.S., Estabrook, K., Hsieh, E.J., Keane, C.J., Montgomery, D.S. & Phillion, D.W. (1995). Characterization of titanium laser-produced plasmas. *Phys. Plasmas* **2**, 3792–3803.

Celliers, P., Da Silva, L.B., Dane, C.B., Mrowka, S., Norton, M., Harder, J., Hackel, L., Matthews, D.L., Fiedorowicz, H., Bartnik, A., Maldonado, J.R. & Abate, J.A. (1996). Optimization of X-ray sources for proximity lithography produced by a high average power Nd:glass laser. *J. Appl. Phys.* **79**, 8258–8268.

Chase, L.F., Jordan, W.C., Perez, J.D. & Pronko, J.G. (1977). Angular distributions of X-ray line radiation from a laser-produced plasma. *Appl. Phys. Lett.* **30**, 137–139.

Deng, X., Liang, X., Chen, Z., Yu, W. & Ma, R. (1986). Uniform illumination of large targets using a lens array. *Appl. Opt.* **25**, 377–381.

Dunn, J., Young, B.K.F., Osterheld, A.L., Foord, M.E., Walling, R.S. & Stewart, R.E. (1995). Spectroscopic investigations of hard X-ray emission from 120-ps laser-produced plasmas at intensities near 10^{17} W cm^{-2}. *Proc. SPIE* **2523**, 254–263.

Eidmann, K. & Schwanda, W. (1991). Conversion of laser light into soft X rays with 3-ns and 30-ps laser pulses. *Laser Part. Beams* **9**, 551–562.

Fabbro, R., Max, C. & Fabre, E. (1985). Planar laser-driven ablation: Effect of inhibited electron thermal conduction. *Phys. Fluids* **28**, 1463–1481.

Faenov, A.Y., Magunov, A.I., Pikuz, T.A., Skobelev, I.Y., Gasilov, S.V., Stagira, S., Calegari, F., Nisoli, M., De Silvestri, S., Poletto, L., Villoresi, P. & Andreev, A.A. (2007). X-ray spectroscopy observation of fast ions generation in plasma produced by short low-contrast laser pulse irradiation of solid targets. *Laser Part. Beams* **25**, 267–275.

Fiedorowicz, H. (2005). Generation of soft X-rays and extreme ultraviolet (EUV) using a laser-irradiated gas puff target. *Laser Part. Beams* **23**, 365–373.

Filevich, J., Rocca, J.J., Jankowska, E., Hammarsten, E.C., Kanizay, K., Marconi, M.C., Moon, S.J. & Shlyaptsev, V.N. (2003). Two-dimensional effects in laser-created plasmas measured with soft-X-ray laser interferometry. *Phys. Rev. E* **67**, 056409.

Fournier, K.B., Constantin, C., Poco, J., Miller, M.C., Back, C.A., Suter, L.J., Satcher, J., Davis, J. & Grun, J. (2004). Efficient multi-keV X-ray sources from Ti-doped aerogel targets. *Phys. Rev. Lett.* **92**, 165005.

Fournier, K.B., Constantin, C., Back, C.A., Suter, L., Chung, H.-K., Miller, M.C., Froula, D.H., Gregori, G., Glenzer, S.H., Dewald, E.L. & Landen, O.L. (2006). Electron-density scaling of conversion efficiency of laser energy into L-shell X-rays. *J. Quant. Spect. Rad. Tran.* **99**, 186–198.

Girard, F., Jadaud, J.P., Naudy, M., Villette, B., Babonneau, D., Primout, M., Depierreux, S., Miller, M.C., Kauffman, R.L., Suter, L.J., Fournier, K.B., Glenzer, S.H., Back, C., Grun, J. & Davis, J. (2004). Multi-keV X-ray conversion from prepulsed foil experiments. *Proc. SPIE* **5196**, 220–233.

Girard, F., Jadaud, J.P., Naudy, M., Villette, B., Babonneau, D., Primout, M., Miller, M.C., Kauffman, R.L., Suter, L.J., Grun, J. & Davis, J. (2005). Multi-keV X-ray conversion efficiencies of laser-preexploded titanium foils. *Phys. Plasmas* **12**, 092705.

Glendinning, S.G., Amendt, P., Budil, K.S., Hammel, B.A., Kalantar, D.H., Key, M.H., Landen, O.L., Remington, B.A. & Desenne, D.E. (1995). Laser plasma diagnostics of dense plasmas. *Proc. SPIE* **2523**, 29–39.

Glenzer, S.H., Gregori, G., Lee, R.W., Rogers, F.G., Pollaine, S.W. & Landen, O.L. (2003). Demonstration of spectrally resolved X-ray scattering in dense plasmas. *Phys. Rev. Lett.* **90**, 175002.

Glibert, K.M., Anthes, J.P., Gusinow, M.A. & Palmer, M.A. (1980). X-ray yields of plasmas heated by 8-nsec neodymium laser pulses. *J. Appl. Phys.* **51**, 1449–1451.

Griem, H.R. (1997) *Principles of Plasma Spectroscopy*. New York: Cambridge University Press.

Higashiguchi, T., Kawasaki, K., Sasaki, W. & Kubodera, S. (2006). Enhancement of extreme ultraviolet emission from a lithium plasma by use of dual laser pulses. *Appl. Phys. Lett.* **88**, 161502.

Hu, G.Y., Liu, S.Y., Zheng, J., Wu, C.S., Li, J.H., Wu, S.C., Zhang, J.Y., Yang, J.M., Yang, G.H., Yi, R.Q., Du, H.B., Huang, Y.X., Hu, X. & Ding, Y.K. (2007). Efficient K-shell X-ray sources produced with titanium foils. *Phys. Plasmas* **14**, 033103.

Hu, G.Y., Zheng, J., Shen, B.F., Lei, A.L., Liu, S.Y., Zhang, J.Y., Yang, J.M., Yang, G.H., Ding, Y.K., Hu, X., Huang, Y.X., Du, H.B., Yi, R.Q. & Xu, Z.Z. (2008). Characterization of a multi-keV X-ray source produced by nanosecond laser irradiation of a solid target: The influence of laser focus spot and target thickness. *Phys. Plasmas* **15**, 023103.

Kalantar, D.H., Haan, S.W., Hammel, B.A., Keane, C.J., Landen, O.L. & Munro, D.H. (1997). X-ray backlit imaging measurement of in-flight pusher density for an indirect drive capsule implosion. *Rev. Sci. Instrum.* **68**, 814–816.

Kauffman, R.L. (1991) X-ray radiation from laser plasma. In *Handbook of Plasma Physics* (Rubenchik A.M. and S. Witkowski S, Eds.). Amsterdam: Elsevier.

Kodama, R., Okada, K., Ikeda, N., Mineo, M., Tanaka, K.A., Mochizuki, T. & Yamanaka, C. (1986). Soft X-ray emission from ω_0, $2\omega_0$, and $4\omega_0$ laser-produced plasmas. *J. Appl. Phys.* **59**, 3050–3052.

Kodama, R., Mochizuki, T., Tanaka, K.A. & Yamanaka, C. (1987). Enhancement of keV X-ray emission in laser-produced plasmas by a weak prepulse laser. *Appl. Phys. Lett.* **50**, 720–722.

Labate, L., Cecchetti, C.A., Galimberti, M., Giulietti, A., Giulietti, D. & Gizzi, L.A. (2005). Detailed characterization of the early X-ray emission of a plasma produced by point-like laser irradiation of solid Al targets. *Phys. Plasmas* **12**, 083101.

Limpouch, J., Renner, O., Krousky, E., Uschmann, I., Forster, E., Kalashnikov, M.P. & Nickles, P.V. (2002). Line X-ray emission from Al targets irradiated by high-intensity variable-length laser pulses. *Laser Part. Beams* **20**, 43–49.

Lin, Z., Deng, X., Fan, D., Wang, S., Chen, S., Zhu, J., Qian, L., Shen, X., Xu, F., Zhu, J., Ma, W., Xie, X., Zheng, Y., Zhang, W., Chen, Q., Ling, M., Huang, H. & Zhang, J. (1999). SG-II laser elementary research and precision SG-II program. *Fusion Eng. Des.* **44**, 61–66.

Mattews, D.L., Campbell, E.M., Ceglio, N.M., Hermes, G., Kauffman, R., Koppel, L., Lee, R., Manes, K., Rupert, V., Slivinshy, V.W., Turner, R. & Ze, F. (1983). Characterization of laser-produced plasma X-ray sources for use in X-ray radiography. *J. Appl. Phys.* **54**, 4260–4268.

Max, C.E. (1982) Physics of the coronal plasma in laser fusion targets. In *Laser-Plasma Interaction* (Balian R and J. C. Adam J.C., Eds). Amsterdam: North-Holland.

Mead, W.C., Campbell, E.M., Estabrook, K.G., Turner, R.E., Kruer, W.L., Lee, P.H.Y., Pruett, B., Rupert, V.C., Tirsell, K.G., Stradling, G.L., Ze, F., Max, C.E. & Rosen, M.D. (1981). Laser-plasma interactions at 0.53 μm for disk targets of varying Z. *Phys. Rev. Lett.* **47**, 1289–1292.

Mead, W.C., Campbell, E.M., Estabrook Kent, Turner, R.E., Kruer, W.L., Lee, P.H.Y., Pruett, B., Rupert, V.C., Tirsell, K.G., Stradling, G.L., Ze, F., Max, C.E., & Lasinski, B.F., (1983). Laser irradiation of disk targets at 0.53 μm wavelength. *Phys. Fluids* **26**, 2316–2331.

Mochizuki, T. & Yamanaka, C. (1986). Efficient soft X-ray generated in short wavelength laser produced plasmas. *Proc. SPIE* **733**, 23–27.

Montgomery, D.S., Landen, O.L., Drake, R.P., Estabrook, K.G., Baldis, H.A., Bradley, S.H. & Procassini, R.J. (1994). Measurements of radial heat wave propagation in laser-produced exploding-foil plasmas. *Phys. Rev. Lett.* **73**, 2055–2058.

Pelletier, J.F., Chaker, M. & Kieffer, J.C. (1997). Soft X-ray emission produced by a sub-picosecond laser in a single- and double-pulse scheme. *J. Appl. Phys.* **81**, 5980–5983.

Peng, H.S., Zhang, X.M., Zheng, W.G., Wei, X.F., Huang, X.J., Sui, Z., Jing, F., Zhu, J., Zhu, Q.H., Wang, X.D., Zhou, K.N., Liu, L.Q., Zeng, X.M., Wang, X., Zhu, J.Q., Lin, Z.Q. & Zhang, W.Y. (2006). High-power solid-state lasers for high-energy-density physics applications at CAEP. *Proc. SPIE* **6344**, 634402.

Phillion, D.W. & Hailey, C.J. (1986). Brightness and duration of X-ray line sources irradiated with intense 0.53-μm laser light at 60 and 120 ps pulse width. *Phys. Rev. A* **34**, 4886–4896.

Pikuz, T.A., Faenov, A.Ya, Fraenkel, M.A., Zigler, Flora, F., Bollanti, S., Dilazzaro, P., Letardi, T., Grilli, A., Palladino, L., Tomassetti, G., Reale, A., Reale, L., Scafati, A., Limongi, T., Bonfigli, F., Alainelli, L. & Sanchez, Del Rio M. (2002). Shadow monochromatic backlighting: Large-field high resolution X-ray shadowgraphy with improved spectral tenability. *Laser Part. Beams* **19**, 285–293.

Primout, M. (2005). Optimization of X-ray conversion efficiency of laser preformed metallic plasma. *J. X-ray Sci. Technol.* **13**, 23–36.

Rafique, M.S., Khaleeq-Ur-Rahman, M., Riaz, I., Jalil, R. & Farid, N. (2008). External magnetic field effect on plume images and X-ray emission from a nanosecond laser produced plasma. *Laser Part. Beams* **26**, 217–224.

Riley, D., Weaver, I., McSherry, D., Dunne, M., Neely, D., Notley, M. & Nardi, E. (2002*a*). Direct observation of strong coupling in a dense plasma. *Phys. Rev. E* **66**, 046408.

Riley, D., Woolsey, N.C., McSherry, D., Khattak, F.Y. & Weaver, I. (2002*b*). He-like X-ray line emission from laser irradiated sources. *Plasma Sour. Sci. Technol.* **11**, 484–491.

Riley, D., Khattak, F.Y., Garcia Saiz, E., Gregori, G., Bandyopadhyay, S., Notley, M., Neely, D., Chambers, D., Moore, A. & Comley, A. (2007). Spectrally resolved X-ray scatter from laser-shock-driven plasmas. *Laser Part. Beams* **25**, 465–469.

Ruggles, L.E., Porter, J.L., Rambo Jr., P.K., Simpson, W.W., Vargas, M.F., Bennett, G.R. & Smith, I.C. (2003). Measurements of 4–10 keV X-ray production with the Z-Beamlet laser. *Rev. Sci. Instrum.* **74**, 2206–2210.

Schollmeier, M., Rodriguez Prieto, G., Rosmej, F.B., Schaumann, G., Blazevic, A., Rosmej, O.N. & Roth, M. (2006). Investigation of laser-produced chlorine plasma radiation for non-monochromatic X-ray scattering experiments. *Laser Part. Beams* **24**, 335–345.

Schollmeier, M., Becker, S., Geissel, M., Flippo, K.A., Blazevic, A., Gaillard, S.A., Gautier, D.C., Gruner, F., Harres, K., Kimmel, M., Nurnberg, F., Rambo, P., Schramm, U., Schreiber, J., Schutrumpf, J., Schwarz, J., Tahir, N.A., Atherton, B., Habs, D., Hegelich, B.M. & Roth, M. (2008). Controlled transport and focusing of laser-accelerated protons with miniature magnetic devices. *Phys. Rev. Lett.* **101**, 055004.

Scott, J.M., Beck, J.B., Batha, S.H., Barnes, C.W. & Tubbs, D.L. (2001). Radiographic image analysis of cylindrical implosion experiments (invited). *Rev. Sci. Instrum.* **72**, 643–650.

Tahir, N.A., Udrea, S., Deutsch, C., Fortov, V.E., Grandjouan, G., Gryaznov, V., Hoffmann, D.H.H., Hulsmann, P., Kirk, M., Lomonosov, I.V., Piriz, A.R., Shutov, A., Spiller, P., Temporal, M. & Varentsov, D. (2004). Target heating in high-energy-density matter experiments at the proposed GSI FAIR facility: Non-linear bunch rotation in SIS 100 and

optimization of spot size and pulse length. *Laser Part. Beams* **22**, 485–493.

Tahir, N.A., Spiller, P., Shutov, A., Lomonosov, I.V., Gryaznov, V., Piriz, A.R., Wouchuk, G., Deutsch, C., Fortov, V.E., Hoffmann, D.H.H. & Schmidt, R. (2007). HEDgeHOB: High-energy density matter generated by heavy ion beams at the future facility for antiprotons and ion research. *Nucl. Instr. Meth. Meth. A* **577**, 238–249.

Teubner, U., Kuhnle, G. & Schafer, F.P. (1991). Soft X-ray spectra produced by subpicosecond laser-double-pulses. *Appl. Phys. Lett*. **59**, 2672–2674.

Von Der Linde, D., Sokolowski-Tinten, K., Blome, CH., Dietrich, C., Zhou, P., Tarasevitch, A., Cavalleri, A., Siders, C.W., Barty, C.P.J., Squier, J., Wilson, K.R., Uschmann, I. & Forster, E. (2001). Generation and application of ultrashort X-ray pulses. *Laser Part. Beams* **19**, 15–22.

Wong, C.S., Woo, H.J. & Yap, S.L. (2007). A low energy tunable pulsed X-ray source based on the pseudospark electron beam. *Laser Part. Beams* **25**, 497–502.

Workman, J. & Kyrala, G.A. (2001*a*). X-ray yield scaling studies performed on the OMEGA laser. *Rev. Sci. Instrum*. **72**, 678–681.

Workman, J. & Kyrala, G.A. (2001*b*). Scaling of X-ray K-shell sources from laser-solid interactions. *Proc. SPIE* **4504**, 168–179.

Workman, J., Lanier, N.E. & Kyrala, G.A. (2003). Analysis of Ti K-shell emission produced from solid targets using nanosecond pulses on the TRIDENT laser facility. *Rev. Sci. Instrum*. **74**, 2165–2168.

Yaakobi, B., Bourke, P., Conturie, Y., Delettrez, J., Forsyth, J.M., Frankel, R.D., Goldman, L.M., McCrory, R.L., Seka, W. & Soures, J.M. (1981). High X-ray conversion efficiency with target irradiation by a frequency tripled Nd: Glass laser. *Opt. Commun*. **38**, 196–200.

https://doi.org/10.1017/S0263034608000682 Published online by Cambridge University Press